

10-1-2010

Pseudogap and its critical point in the heavily doped Ba(Fe_{1-x}Co_x)₂As₂ from c-axis resistivity measurements

Makariy A. Tanatar

Iowa State University and Ames Laboratory, tanatar@ameslab.gov

Ni Ni

Iowa State University and Ames Laboratory

Alexander N. Thaler

Iowa State University and Ames Laboratory

Sergey L. Bud'ko

Iowa State University and Ames Laboratory, budko@ameslab.gov

Paul C. Canfield

Iowa State University and Ames Laboratory, canfield@ameslab.gov

See next page for additional authors

Follow this and additional works at: https://lib.dr.iastate.edu/physastro_pubs



Part of the [Condensed Matter Physics Commons](#)

The complete bibliographic information for this item can be found at https://lib.dr.iastate.edu/physastro_pubs/690.
For information on how to cite this item, please visit <http://lib.dr.iastate.edu/howtocite.html>.

This Article is brought to you for free and open access by the Physics and Astronomy at Iowa State University Digital Repository. It has been accepted for inclusion in Physics and Astronomy Publications by an authorized administrator of Iowa State University Digital Repository. For more information, please contact digirep@iastate.edu.

Pseudogap and its critical point in the heavily doped $\text{Ba}(\text{Fe}_{1-x}\text{Co}_x)_2\text{As}_2$ from c-axis resistivity measurements

Abstract

Temperature-dependent interplane resistivity, $\rho(c)(T)$, was used to characterize the normal state of the iron-arsenide superconductor $\text{Ba}(\text{Fe}_{1-x}\text{Co}_x)_2\text{As}_2$ over a broad doping range $0 \leq x \leq 0.50$. The data were compared with in-plane resistivity, $\rho(a)(T)$, and magnetic susceptibility, $\chi(T)$, taken in H perpendicular to c , as well as Co NMR Knight shift, K_{59} , and spin-relaxation rate, $1/T_1T$. The interplane resistivity data show a clear correlation with the NMR Knight shift, assigned to the formation of the pseudogap. Evolution of $\rho(c)(T)$ with doping reveals two characteristic energy scales. The temperature of the crossover from nonmetallic, increasing on cooling, behavior of $\rho(c)(T)$ at high temperatures to metallic behavior at low temperatures, T^* , correlates well with an anomaly in all three magnetic measurements. This characteristic temperature, equal to approximately 200 K in the parent compound, $x = 0$, decreases with doping and vanishes near x^* approximate to 0.25. For doping levels $x \geq 0.166$, an additional feature appears above T^* with metallic behavior of $\rho(c)(T)$ found above the low-temperature resistivity increase. The characteristic temperature of this charge-gap formation, T_{CG} , vanishes at $x(\text{CG})$ similar or equal to 0.30, paving the way to metallic, T linear, $\rho(c)(T)$ close to $x(\text{CG})$ and superlinear T dependence for $x > x(\text{CG})$. None of these features are evident in the in-plane resistivity $\rho(c)(T)$. For doping levels $x < x(\text{CG})$, $\chi(T)$ shows a known, anomalous, T -linear dependence, which disappears for $x > x(\text{CG})$. These features are consistent with the existence of a charge gap, accompanying formation of the magnetic pseudogap, and its critical suppression with doping. The inferred c-axis charge gap reflects the three-dimensional character of the electronic structure and of the magnetism in the iron arsenides.

Disciplines

Condensed Matter Physics

Comments

This article is published as Tanatar, M. A., Ni Ni, A. Thaler, S. L. Bud'ko, P. C. Canfield, and R. Prozorov. "Pseudogap and its critical point in the heavily doped $\text{Ba}(\text{Fe}_{1-x}\text{Co}_x)_2\text{As}_2$ from c-axis resistivity measurements." *Physical Review B* 82, no. 13 (2010): 134528. DOI: [10.1103/PhysRevB.82.134528](https://doi.org/10.1103/PhysRevB.82.134528). Posted with permission.

Authors

Makariy A. Tanatar, Ni Ni, Alexander N. Thaler, Sergey L. Bud'ko, Paul C. Canfield, and Ruslan Prozorov

Pseudogap and its critical point in the heavily doped $\text{Ba}(\text{Fe}_{1-x}\text{Co}_x)_2\text{As}_2$ from c -axis resistivity measurements

M. A. Tanatar,^{1,*} N. Ni,^{1,2} A. Thaler,^{1,2} S. L. Bud'ko,^{1,2} P. C. Canfield,^{1,2} and R. Prozorov^{1,2}

¹*Ames Laboratory, Ames, Iowa 50011, USA*

²*Department of Physics and Astronomy, Iowa State University, Ames, Iowa 50011, USA*

(Received 10 June 2010; revised manuscript received 17 August 2010; published 21 October 2010)

Temperature-dependent interplane resistivity, $\rho_c(T)$, was used to characterize the normal state of the iron-arsenide superconductor $\text{Ba}(\text{Fe}_{1-x}\text{Co}_x)_2\text{As}_2$ over a broad doping range $0 \leq x < 0.50$. The data were compared with in-plane resistivity, $\rho_a(T)$, and magnetic susceptibility, $\chi(T)$, taken in $H \perp c$, as well as Co NMR Knight shift, ^{59}K , and spin-relaxation rate, $1/T_1T$. The interplane resistivity data show a clear correlation with the NMR Knight shift, assigned to the formation of the pseudogap. Evolution of $\rho_c(T)$ with doping reveals two characteristic energy scales. The temperature of the crossover from nonmetallic, increasing on cooling, behavior of $\rho_c(T)$ at high temperatures to metallic behavior at low temperatures, T^* , correlates well with an anomaly in all three magnetic measurements. This characteristic temperature, equal to approximately 200 K in the parent compound, $x=0$, decreases with doping and vanishes near $x^* \approx 0.25$. For doping levels $x \geq 0.166$, an additional feature appears above T^* with metallic behavior of $\rho_c(T)$ found above the low-temperature resistivity increase. The characteristic temperature of this charge-gap formation, T_{CG} , vanishes at $x_{\text{CG}} \approx 0.30$, paving the way to metallic, T linear, $\rho_c(T)$ close to x_{CG} and superlinear T dependence for $x > x_{\text{CG}}$. None of these features are evident in the in-plane resistivity $\rho_a(T)$. For doping levels $x < x_{\text{CG}}$, $\chi(T)$ shows a known, anomalous, T -linear dependence, which disappears for $x > x_{\text{CG}}$. These features are consistent with the existence of a charge gap, accompanying formation of the magnetic pseudogap, and its critical suppression with doping. The inferred c -axis charge gap reflects the three-dimensional character of the electronic structure and of the magnetism in the iron arsenides.

DOI: [10.1103/PhysRevB.82.134528](https://doi.org/10.1103/PhysRevB.82.134528)

PACS number(s): 74.70.Dd, 72.15.-v, 74.25.Jb

The metallic state of the, until recently, only known high-temperature superconductors, the compounds based of Cu-O elements and frequently referred to as the cuprates,¹ is characterized by a plethora of anomalies. At low doping levels, anomalous behaviors are found in the temperature-dependent resistivity, magnetization, NMR Knight shift, and relaxation rate, as well as in spectroscopic data.² These behaviors are consistent with a decrease in the density of states (DOS) at low temperatures, usually assigned with pseudogap formation. In the definition of the pseudogap we follow Timusk and Statt,² who wrote “By a pseudogap we mean a partial gap. An example of such a partial gap would be a situation where, within the band-theory approximation, some regions of the Fermi surface become gapped while other parts retain their conducting properties and with increased doping the gapped portion diminishes and the materials become more metallic.” The phenomenology and k -space distribution of the pseudogap in the cuprates is now well established,³ however, its microscopic origin is still debated.⁴ Main theories and experiments link it to two neighboring phases, an anti-ferromagnetic Mott insulator, with pseudogap arising due to exotic magnetism,⁵ or to a superconducting phase, as an effect of the preformed superconducting pairs.⁶ The pseudogap is universally observed in both hole- and electron-doped⁷ cuprates, though it is much more pronounced in the former.

Discovery of superconductivity with high critical temperatures in FeAs-based materials,⁸ breaking the monopoly of the cuprates, naturally raises the question about the common features of the two families.⁹ It fuels the hopes that one day the enigmatic mechanism of high-temperature superconductivity will be understood. One of the important features to

understand from such comparison, is a possible link between superconductivity and the pseudogap.

Features consistent with pseudogap are indeed observed in the hole-doped RFeAsO (Refs. 10–14) (R =rare earth, 1111 compounds in the following). A clearly decreased density of states is found in Angular Resolved Photo Emission Spectroscopy (ARPES) measurements in $(\text{Ba},\text{K})\text{Fe}_2\text{As}_2$ (BaK122 compounds in the following).¹⁵ Because the parent compounds of iron pnictides are metals, the pseudogap here is believed to arise from nesting instability.¹⁶

On the contrary, the experimental situation in electron-doped $\text{Ba}(\text{Fe}_{1-x}\text{Co}_x)_2\text{As}_2$ (BaCo122 in the following) is less clear. NMR studies suggest the existence of a pseudogap over the whole doping range, from magnetically ordered parent compound to overdoped superconductor. This is revealed as a temperature-dependent Knight shift K , well described by an activation formula $K=A+B \exp(-T_{\text{PG}}/T)$, where $T_{\text{PG}} \equiv \Delta_{\text{PG}}/k_B$ can be determined from a fit as $560 \text{ K} \pm 150 \text{ K}$ at optimal doping.¹⁷ Since Knight shift and static magnetic susceptibility are closely related, this should be linked to anomalous T -linear susceptibility. In contrast, ARPES found a tiny feature just above the superconducting T_c (Ref. 18) whereas the in-plane resistivity does not reveal any pseudogaplike features¹⁹ and is well described in a broad composition range by a sum of T linear and T^2 contributions.²⁰

We have recently undertaken extensive anisotropic electrical resistivity measurements on parent and optimally doped $\text{Ba}(\text{Fe}_{1-x}\text{Co}_x)_2\text{As}_2$.^{21–23} In addition to a small ac anisotropy, we found different temperature dependencies of the in-plane and interplane electrical resistivity. Here we report a

systematic study of the evolution of the interplane resistivity with doping. We show that the anomalies in the interplane resistivity reflect the existence of the enigmatic pseudogap state in BaCo122. Clear correlation with NMR measurements in BaCo122 as a function of doping²⁴ and the lack of any associated features in the in-plane transport, suggest uniaxial symmetry of the pseudogap.

Tracking the evolution of the characteristic features of the temperature-dependent interplane resistivity with doping we found a critical concentration, $x_{CG} \approx 0.30$, beyond which the pseudogap features disappear. Our magnetization measurements show that this corresponds to the concentration at which the magnetic susceptibility loses its anomalous T linear increase at high temperatures. At the critical concentration, the $\rho_c(T)$ is very close to linear. This evolution of the interplane electrical resistivity suggests a (quantum) critical point^{20,25} on the edge of the pseudogap state.

I. EXPERIMENTAL

Single crystals of BaFe₂As₂ doped with Co were grown from a starting load of metallic Ba, FeAs, and CoAs, as described in detail elsewhere.¹⁹ Crystals were thick platelets with sizes as big as $12 \times 8 \times 1$ mm³ and large faces corresponding to the tetragonal (001) plane. The actual content of Co in the crystals was determined with wavelength dispersive spectroscopy (WDS) electron probe microanalysis and is the $x \equiv x_{WDS}$ value used throughout this text.

In our study of resistivity anisotropy in Ba(Fe_{1-x}Co_x)₂As₂, undoped $x=0$ (Ref. 22) and optimally doped $x=0.074$ (Ref. 21), we have found that special care must be taken for measurements in configurations with current along the tetragonal c axis so as to avoid effects associated with the exfoliation of the samples. Cutting and shaping into transport samples inevitably introduces cracks, which affect the effective geometric factors of the samples and, in case the cracks are deep, can produce admixture of the in-plane resistivity component. A strong tendency to exfoliate prevents the cutting of samples with $c \gg a$. This limitation puts severe constraints on the measurement technique.

Samples for electrical resistivity measurements with current flow along the tetragonal c axis (ρ_c) were cut into $(0.3-0.7) \times (0.3-0.7) \times (0.1-0.5)$ mm³ ($a \times b \times c$) slabs. All sample dimensions were measured with an accuracy of about 10%. Contacts to the samples were made by attaching silver wires using ultrapure tin, resulting in an ultralow contact resistance (less than 10 $\mu\Omega$).²⁶ Measurements of ρ_c were made in the two-probe sample configuration. Contacts were covering the whole ab plane area of the c -axis samples. A four-probe scheme was used to measure the resistance down to the contact to the sample, i.e., the sum of the actual sample resistance R_s and contact resistance R_c was measured. Taking into account that $R_s \gg R_c$, contact resistance represents a minor correction on the order of 1–5 %. This can be directly seen for superconducting samples^{21,26,27} at temperatures $T < T_c$, where $R_s=0$ and the measured resistance represents R_c .

Two probe resistivity measurements have one important advantage over commonly used in highly anisotropic mate-

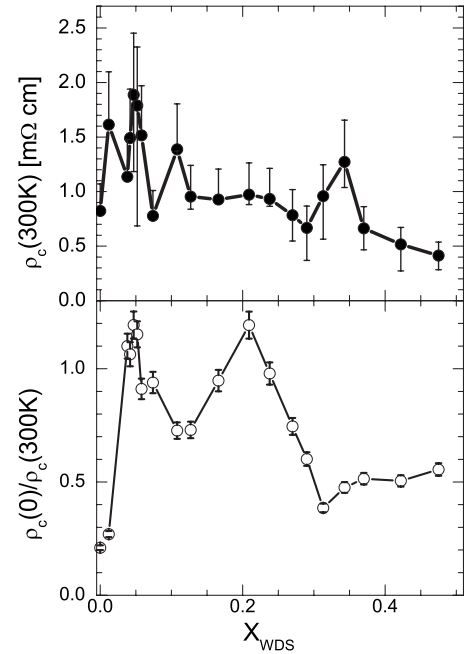


FIG. 1. Room-temperature interplane resistivity, $\rho_c(300 \text{ K})$, of Ba(Fe_{1-x}Co_x)₂As₂ as a function of doping (top panel). Lower panel shows doping dependence of the ratio of resistivities at low temperatures and at room temperature, $\rho_c(0)/\rho_c(300 \text{ K})$.

rials technique, in which measurements are performed in four-probe scheme with both current and potential contacts located on conducting ab plane. Here the potential contacts stay off the current path and if the anisotropy is not high, can lead to spurious temperature dependencies due to the variation of anisotropy and thus the redistribution of current flow within the sample.²⁸ As we have shown in our preceding studies on optimally doped²¹ and parent²² compositions, comparison of rigorous measurements using Montgomery technique and two-probe measurements gives identical temperature dependence.

The drawback of the measurement on samples with $c \gg a$ is that any inhomogeneity in the contact resistivity or internal sample connectivity admixes in-plane component due to redistribution of the current. To minimize this effect, we performed measurements of ρ_c on at least five samples of each compositions. In all cases we obtained qualitatively similar temperature dependences of the electrical resistivity, as represented by the ratio of resistivities at room and low temperatures, $\rho_c(0)/\rho_c(300)$. The resistivity value, however, showed a notable scatter and at room temperature was typically in the range 1–2 $m\Omega \text{ cm}$. For the sake of comparison we selected the samples with the temperature dependence of resistivity least similar to that of $\rho_a(T)$. The value of resistivity for these samples at room temperature is shown as a function of doping in the top panel of Fig. 1. Typically, these samples had the lowest value of electrical resistivity, as described in detail in Ref. 21. This is important since partial exfoliation increases resistivity values.²¹ As a best demonstration of the correctness of our measurements, thermal conductivity measurements in the normal state for samples with $x=0.127$, accessed by the application of magnetic field, found Wiedemann-Franz law to be obeyed in $T \rightarrow 0$ limit.²⁹

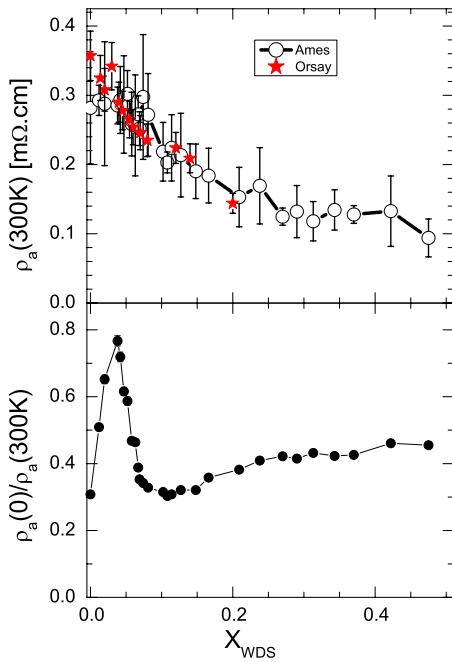


FIG. 2. (Color online) Room-temperature in-plane resistivity, $\rho_a(300\text{ K})$, of $\text{Ba}(\text{Fe}_{1-x}\text{Co}_x)_2\text{As}_2$ as a function of doping (top panel). Red stars show resistivity values taken from Ref. 31. Lower panel shows doping dependence of the resistivity ratio, $\rho_a(0)/\rho_a(300\text{ K})$.

This *quantitative* coincidence of two independent measurements is very important because cracks can be partially transparent for phonons and thus affect thermal and electrical transport in a different way, leading to gross extrinsic Wiedemann-Franz law violation.³⁰ The evolutions of the interplane resistivity at room temperature, $\rho(300\text{ K})$, and of the residual resistivity ratio, $\rho_c(0)/\rho(300\text{ K})$, with doping are summarized in Fig. 1. The resistivity value at room temperature for most compositions stays in the range 1–1.5 $\text{m}\Omega\text{ cm}$, with doping it decreases to approximately 0.5 $\text{m}\Omega\text{ cm}$. For several x compositions we were not able to find crystals with resistivity values lower than 2 $\text{m}\Omega\text{ cm}$, despite the facts that (1) the evolution of the temperature-dependent resistivity for these samples followed the general trend and (2) close in x compositions show usual resistivity values. This limits the accuracy of the absolute ρ_c value determination by approximately a factor of 2.

Samples for electrical resistivity measurements with current flow along the $[100]$ a axis in the tetragonal plane (ρ_a) were cut into bars of $(2-3) \times (0.1-0.2) \times (0.1-0.2)\text{ mm}^3$ ($a \times b \times c$). Measurements of ρ_a were made in both standard four-probe and two-probe configurations, and gave identical results, see Refs. 26 and 27. Electrical resistivity of the samples at room temperature is shown as a function of doping in Fig. 2. Error bars represent statistical standard deviation for at least five samples of each composition. The in-plane resistivity monotonically decreases from 270 $\mu\Omega\text{ cm}$ in the parent compound to about 100 $\mu\Omega\text{ cm}$ in the heavily overdoped composition with $x=0.48$. The magnitude of $\rho_a(300)$ is in good agreement with previous report over a narrower doping range.³¹ Residual

resistivity ratio shows a rapid increase in the range, where the Fermi surface topology change (Lifshitz transition) happens (at $x \approx 0.025$),^{32,33} reaches a maximum at $x=0.05$ and then decreases toward minimum close to $x=0.1$. With further doping the ratio increases, the effect which mainly comes from a decrease in resistivity at room temperature.

The magnetization measurements were performed on cleaved samples to minimize the risk from small amount of surface flux. Samples typically had total mass of 10–20 mg. Measurements were performed in a standard *MPSM* superconducting quantum interference device magnetometer in a field of 5 T. Unless specially mentioned, magnetization measurements were performed in configuration $H \perp c$. For a composition $x=0.343$ measurements were also performed with $H \parallel c$. They found essentially no anisotropy, similar to our previous study.¹⁹

II. RESULTS

In Figs. 3 and 4 we present evolution of the temperature-dependent resistivity with doping. The interplane resistivity (top panel, Fig. 3) of the parent compound decreases sharply below the temperature of the coupled structural/magnetic transition, T_{SM} , similar to the in-plane resistivity (bottom panel, Fig. 3). In the interplane resistivity the decrease at $T_{SM}=135\text{ K}$ is preceded with resistivity maximum at $T^* \approx 200\text{ K}$ (shown with arrow in Fig. 3). With doping, the decrease of $\rho_c(T)$ below T_{SM} turns into an increase (as seen for samples with $x=0.038-0.058$), similar to the behavior of $\rho_a(T)$, which shows two anomalies at the temperatures of split with doping structural, T_S , and magnetic, T_M , transitions.¹⁹ This change near $x \approx 0.025$ is consistent with the proposed Lifshitz transition (Fermi surface topology change) as seen in thermoelectric power, Hall-effect measurements³² and ARPES.³³ However, the maximum in $\rho_c(T)$ at T^* remains of the same crossover type and does not follow resistivity behavior below T_{SM} (either increase or decrease), suggesting that it is an independent feature. At doping close to optimum, $x_{opt} \approx 0.07$, the features due to structural/magnetic transition are completely suppressed [in both $\rho_a(T)$ and $\rho_c(T)$], and the temperature dependence of the interplane resistivity is dominated by the maximum at T^* and superconducting transition.

At the highest doping shown in Fig. 3, $x=0.166$, when the superconductivity is suppressed, a new feature appears in the temperature-dependent interplane resistivity: a shallow resistivity minimum appears at $T_{CG} > T^*$. In Fig. 4 we present the evolution of the resistivity for higher Co concentrations, starting from those on the overdoped side of the superconducting dome, $x=0.127$. The top panel shows the interplane resistivity, the bottom panel shows the in-plane resistivity, which shows metallic behavior for all compositions. Cross arrows in the top panel show the position of the high-temperature crossover from the metallic to nonmetallic temperature dependence of the interplane resistivity at T_{CG} . Cross arrows in the bottom panel show the same characteristic temperatures with respect to the temperature-dependent in-plane resistivity finding no discernible features in the $\rho_a(T)$ curves.

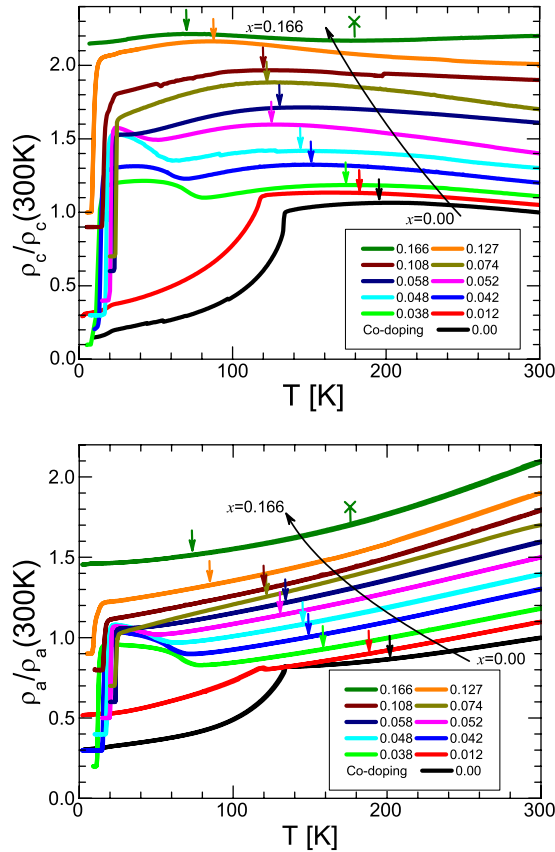


FIG. 3. (Color online) Temperature dependence of the interplane resistivity, ρ_c , normalized by its value at room temperature $\rho_c(300\text{ K})$, for samples of $\text{Ba}(\text{Fe}_{1-x}\text{Co}_x)_2\text{As}_2$ with $x \leq 0.166$ (slightly above the concentration boundary for the superconducting dome) as shown in the figure (top panel). The curves are offset to avoid overlapping. Arrows show a position of the resistivity maximum, presented as a function of dopant concentration in the T - x phase diagram (see Fig. 5 below), cross arrows show position of the resistivity minimum, T_{CG} , appearing at high doping levels. Bottom panel shows doping evolution of the temperature-dependent in-plane resistivity, ρ_a , normalized by room-temperature value $\rho_a(300\text{ K})$. Arrows show positions of T^* and T_{CG} as determined from $\rho_c(T)$, revealing no discernible features in the in-plane resistivity.

We summarize the doping evolution of the main features of the temperature-dependent resistivity in the phase diagram, Fig. 5. The lines of the superconducting, T_c , structural, T_S and magnetic, T_M transitions are discernible in both in-plane¹⁹ and interplane resistivities. The lines corresponding to maxima, T^* , and minima T_{CG} of the temperature-dependent interplane resistivity find no correspondence in the temperature dependence of the in-plane transport.

This phase diagram suggests existence of a critical concentration, at which charge gap vanishes. Interestingly enough, at the concentration close to critical, $x_{CG} \approx 0.30$, the interplane resistivity shows a linear temperature dependence over a broad temperature range, as seen for a sample with $x=0.313$ (red curve in the top panel of Fig. 4) for $T > 20\text{ K}$. For higher x , the temperature-dependent resistivity develops positive curvature, and can be reasonably described by a sum of T -linear and T^2 contributions, $\rho_c(T)$

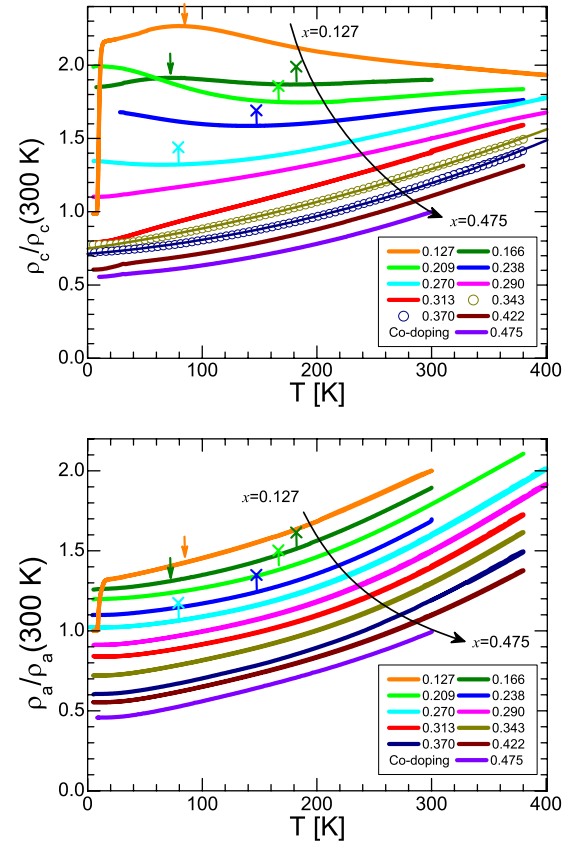


FIG. 4. (Color online) Temperature dependence of the interplane resistivity, ρ_c , normalized by its value at room temperature $\rho_c(300\text{ K})$, for samples of $\text{Ba}(\text{Fe}_{1-x}\text{Co}_x)_2\text{As}_2$ with high doping levels $x \geq 0.127$ as shown in the figure (top panel). The curves are offset to avoid overlapping. Cross arrows and straight arrows show positions of the resistivity minimum, T_{CG} , and maximum, T^* , respectively. Lines with $x=0.343$ and $x=0.370$ curves show a second order polynomial fit through the data, as discussed in the text. Bottom panel shows evolution of the temperature-dependent in-plane resistivity, ρ_a , normalized by room-temperature value $\rho_a(300\text{ K})$. Arrows show positions of T_{CG} and T^* as determined from the interplane resistivity temperature dependence, revealing no discernible features in the in-plane resistivity.

$= \rho_0 + AT + BT^2$, similar to in-plane transport,²⁰ as shown in the top panel of Fig. 3 for samples with $x=0.343$ and $x=0.370$.

In Fig. 6 we compare the interplane resistivity with earlier evidence of the pseudogap in the electron-doped iron arsenides: the temperature dependence of the ^{59}Co NMR Knight shift K and T -normalized NMR relaxation rate, $\frac{1}{T_1 T}$, as measured in Ref. 24. We recall that, in a simple metal, both K and $\frac{1}{T_1 T}$ should be temperature independent. In contrast, both Knight shift and relaxation-rate data in $\text{Ba}(\text{Fe}_{1-x}\text{Co}_x)_2\text{As}_2$ are strongly temperature dependent. In the parent compound, $x=0$, $K(T)$ shows an increase with temperature (seen in all compositions) with a mild slope change around 210 K. On the other hand, $\frac{1}{T_1 T}$ slightly increases on cooling below 200 K on approaching the temperature of the coupled structural-magnetic transition, $T_{SM} = 135\text{ K}$. These two features in $K(T)$ and $\frac{1}{T_1 T}$ vs T are close in temperature to a shallow maximum

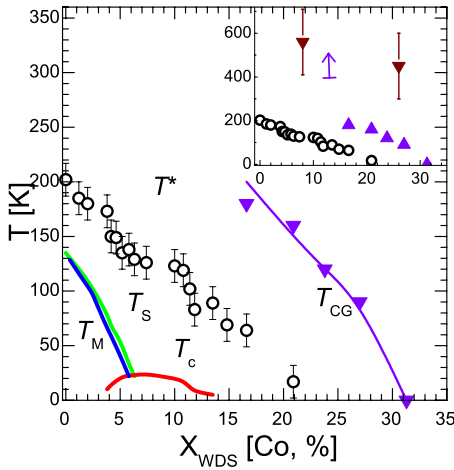


FIG. 5. (Color online) Temperature-doping phase diagram of $\text{Ba}(\text{Fe}_{1-x}\text{Co}_x)_2\text{As}_2$ as determined from interplane resistivity measurements. Inset shows comparison of T^* and T_{CG} , corresponding to the maxima and minima in $\rho_c(T)$ with T_{PG} as found in NMR study by fitting the temperature-dependent Knight shift (Refs. 24 and 34). Arrow in the inset shows a minimum estimate for T_{CG} for the border composition $x=0.127$.

in $\rho_c(T)$ at around 200 K, preceding a sharp drop of resistivity at T_{SM} . They are close to a temperature where anomalous in-plane resistivity anisotropy develops in detwinned single crystals of parent compounds²³ due to nematic order.³⁵

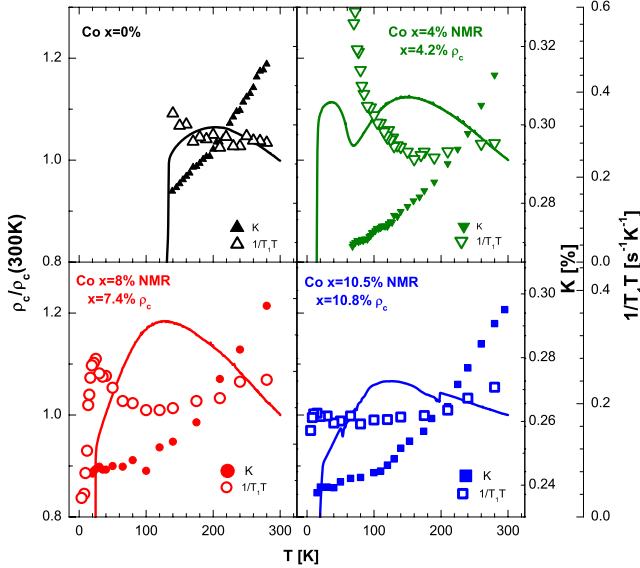


FIG. 6. (Color online) Comparison of the temperature-dependent interplane resistivity ρ_c (solid lines, left scale) with the temperature-dependent ^{59}Co NMR Knight shift $K(T)$ (solid symbols) and relaxation rate, $1/T_1 T$, (open symbols) from Ref. 24 (two right scales) for BaFe_2As_2 (top left panel) and $\text{Ba}(\text{Fe}_{1-x}\text{Co}_x)_2\text{As}_2$ with $x=0.04$ (top right panel), $x=0.074-0.08$ (bottom left panel), and $x=0.105-0.108$ (bottom right panel). A broad maximum in the temperature dependence of the interplane resistivity clearly correlates with pseudogap features in NMR measurements: a crossover slope change in $K(T)$ and the onset of a low-temperature rapid rise in $1/T_1 T$.

This correlation between the features in the temperature-dependent NMR Knight shift and the interplane electrical resistivity becomes clearer with increasing Co doping. The slope change in the Knight shift becomes more pronounced and, for a composition with $x=0.105$, it shifts down to ~ 100 K. In both NMR measurements and in the interplane resistivity the features remain of a broad crossover type with difficult to define characteristic temperatures. The resistivity maximum is a better defined feature though it is still broad and its location for several samples studied for each composition could be slightly affected by the admixture of the in-plane resistivity. This admixture may affect the $\rho_c(T)$ for the $x=0.108$ sample in Fig. 6, as suggested by its slight deviation from the series evolution with doping, top panel in Fig. 3. (Small jumps in the temperature dependence are extrinsic and are caused by sample cracking during thermal cycle.)

The linearly increasing NMR Knight shift³⁶ reflects an unusual linear temperature-dependent static magnetic susceptibility, $\chi(T)$.³⁷⁻³⁹ This anomalous linear $\chi(T)$ dependence was shown to go away at high doping levels, being replaced by a Curie-Weiss behavior of susceptibility.³⁷ The magnitude of the Knight shift variation also diminishes for overdoped compositions and it was suggested that the pseudogap feature disappears at critical concentration for superconductivity $x_{SC} \approx 0.2$.³⁴

We performed magnetization measurements on Co-doped compositions, as shown in Fig. 7. The behavior at low Co dopings $0 < x \leq 0.166$ was studied systematically by Ni *et al.*¹⁹ for both orientations of magnetic field parallel and perpendicular to the tetragonal c axis and found small anisotropy. Our measurements for $x \geq 0.166$ concentrate on doping evolution of susceptibility in configuration $H \perp c$. We performed measurements with $H \parallel c$ only for sample $x=0.343$ and found no anisotropy. As can be seen from Fig. 7, the slope of the T -linear portion in $\chi(T)$ gradually diminishes with x . The $\chi_{mole}(T)$ curve for $x=0.290$ shows very small but still clearly discernible increase with T though with the slope notably smaller than the slope for $x=0.270$. For $x=0.313$ the increase in magnetic susceptibility with temperature is completely gone. Instead, $\chi(T)$ becomes temperature independent above 150 K. The Curie-Weiss increase of $\chi(T)$ on cooling at low temperatures for sample with $x=0.313$ is most likely extrinsic, it is not observed for samples with lower and higher doping, $x=0.290$ and $x=0.343$. On the other hand, the $\chi_{mole}(T)$ dependence does not reveal any increase at high T for both $x=0.313$ and two different samples of $x=0.343$.

To quantify this evolution, in the bottom panel of Fig. 7 we show a slope of $\chi_{mole}(T)$ at $T=250$ K as a function of x . The dependence shows a dramatic change between $x=0.290$ and $x=0.313$, the same concentration as x_{CG} determined from interplane resistivity. We note that since the crystals used in the interplane resistivity and magnetization measurements are from the same batches, there is minimal uncertainty in the concentration comparison. Both interplane resistivity and magnetic susceptibility show pronounced changes of behavior between $x=0.290$ and $x=0.313$. For $x > 0.313$, the interplane resistivity increases monotonically and superlinearly with temperature as expected for a metal. The flat temperature-independent magnetic susceptibility is

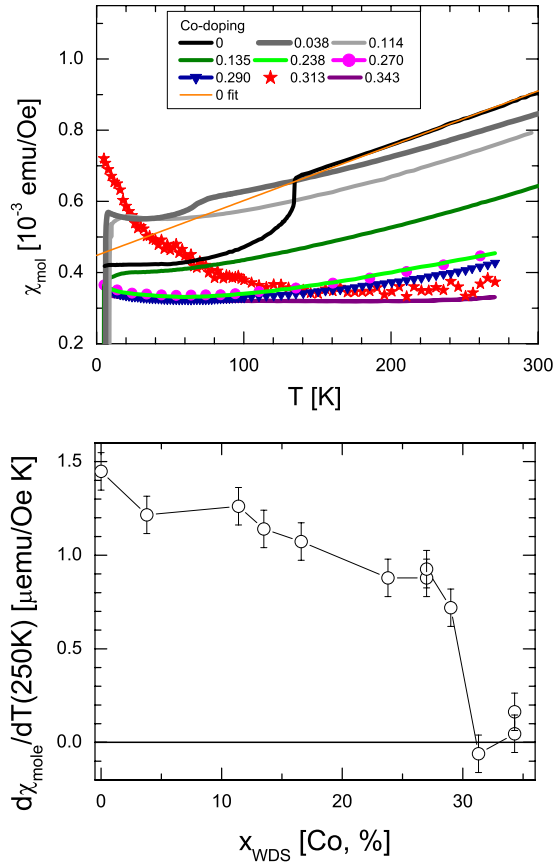


FIG. 7. (Color online) Top panel: temperature-dependent molar magnetic susceptibility, $\chi_{\text{mole}}(T)$, measured in magnetic field $H \perp c = 5$ T. The data for low dopings are from Ref. 19. On doping increase the slope of the T -linear increase in $\chi(T)$ (shown with orange line for pure composition $x=0$ at $T=250$ K) decreases and for $x=0.313$ the dependence becomes flat at $T > \sim 150$ K. Bottom panel: doping evolution of the slope of $\chi_{\text{mole}}(T)$, $d\chi_{\text{mole}}(T)/dT$, at $T=250$ K.

expected for Pauli susceptibility of a metal as well. The disappearance of the linearly rising $\chi(T)$ for heavily doped compositions is similar to the early report³⁷ though with notable difference in the concentration boundaries ($x=0.125$ in our notations vs 0.30). This discrepancy may be a result of poor composition control in early crystals. We would like to point out that at similar concentration ~ 0.4 (there is no systematic doping-evolution study in the range) Hall constant becomes temperature independent, again in line with expectation of the behavior of a usual metal.⁴⁰

III. DISCUSSION

A. Doping evolution of the anisotropy

The electronic structure of Co-doped BaFe_2As_2 is now well established to be three-dimensional by various techniques.^{18,41–44} However, evolution of the anisotropy with doping was never studied in a systematic way. From Fig. 2 we can see that doping in the range from $x=0$ to $x=0.48$ leads to an approximately three times decrease in the in-plane resistivity at room temperature, agreeing,

within error bars, with the previous measurements over narrower doping range.³¹ For ρ_c , Fig. 1, the variation is approximately of the same magnitude, keeping in mind an uncertainty of the factor of 2 for ρ_c values. This suggests that the evolution of the anisotropy in a broad doping range is very gradual and puts an upper bound of about a factor of 2 for the anisotropy change. Comparison of these numbers with the existing band-structure calculations^{21,22,45–48} should be taken with a grain of salt since variation in the position of the As atom in the lattice from the one obtained in experiment to the one calculated from total lattice energy minimum^{21,22} brings the effect which by far exceeds the total anisotropy variation. A general decrease in both in-plane and interplane resistivities with doping is suggestive that charge is actually donated into the system, which does not go in line with suggestions that all doping can be treated as additional scattering.⁴⁸

The anisotropy at low temperatures, important for the anisotropy of the upper critical field in the superconducting state, is heavily affected by the structural/magnetic transition and by the pseudogap. We will discuss these effects in the next sections.

B. Structural/magnetic ordering and interplane resistivity

Magnetic ordering below T_{SM} , presumably of spin-density-wave (SDW) nature,⁴⁹ reconstructs the Fermi surface, opening a SDW gap on electron and hole pockets. This is seen as an increase of the in-plane resistivity in BaCo122 with $x=0.025–0.058$. The parts of the Fermi surface which are not affected by the SDW gap, enjoy a notably reduced inelastic scattering in the magnetically ordered phase.^{23,31,50} In the parent compound, in which elastic scattering is small, this decrease in scattering overcomes the loss of the carrier density so that the total conductivity increases below T_{SM} . Since the interplane transport is determined by the warped parts of the Fermi surface,²¹ affected in a different way by the two-dimensional nesting than cylinders, the interplane resistivity can be affected by much less by the SDW gap opening than ρ_a . This is indeed seen, in BaCo122 , most clearly for sample with $x=0.012$. Here, the in-plane resistivity shows an intermediate behavior between pure and heavier doped compositions: whereas $\rho_a(T)$ increases immediately below T_{SM} and then shows a shallow decrease to a much higher residual value than in pure samples; the interplane resistivity does not manifest a local maximum below T_{SM} and the resistivity decrease is almost as steep as in pure crystals. The features in the temperature-dependent resistivity upon crossing structural and magnetic transitions^{19,51} can be similarly resolved in in-plane and interplane transport, though a feature at the structural transition is always less pronounced in $\rho_c(T)$.

C. Minimum in the temperature-dependent interplane resistivity and charge gap

For our discussion it is important that in the doping range $0.166 < x < 0.313$ resistivity increases on cooling below T_{CG} down to the lowest temperatures while no increase is seen in the in-plane resistivity. Three reasons for resistivity increase

in a metal should be considered. (1) Kondo effect. This involves screening of the local magnetic moments with conduction electron. We do not see any way this effect to be anisotropic. (2) A crossover between incoherent and coherent transport, as observed in the $\text{YBa}_2\text{Cu}_4\text{O}_8$ cuprates (Ref. 28). Low anisotropy values for all dopings, an increase in resistivity with temperature above the minimum for samples with $x > 0.166$, and observation of three-dimensional Fermi surface^{18,41–44} in a variety of measurements for various doping levels do not support this scenario. (3) Actual gap on parts of the Fermi surface (pseudogap). For a reason of continuity of the behavior in the T - x phase space we are forced to assign resistivity decrease above T^* to the onset of quasi-particle activation over the pseudogap.

The importance of charge gap formation for nonmetallic temperature dependence of ρ_c above T^* is most clearly seen from the temperature-dependent interplane resistivity for BaCo122 composition with $0.166 \leq x \leq 0.270$. Here the resistivity shows metallic temperature dependence at high temperatures and then crosses over to a nonmetallic increase below a temperature of a charge gap formation T_{CG} . The monotonic evolution of the curves suggests that for lower dopings, $x < 0.166$, the T_{CG} goes above the experimentally accessible range. If this is true, the end of the temperature range of monotonic resistivity decrease on heating gives us an estimate for a minimum value of charge gap for compositions with $x \leq 0.127$ as above 400 K. In inset in Fig. 5, we compare experimentally determined T_{CG} from the interplane resistivity measurements with T_{PG} determined from fitting $K(T)$ curves. Both measurements have very big error bars and yet they do not match well. This may suggest another possibility, that a metallic temperature dependence of ρ_c at high temperatures is only confined to some range of dopings.

The scenario with the existence of a semimetallic charge gap was invoked for an explanation of the T -linear magnetic susceptibility with simultaneous strong temperature-dependent Hall and Seebeck coefficients.^{31,32,52} In this model thermal activation of carriers over a narrow gap results in a carrier density increase with temperature. This would naturally lead to a decrease of the interplane resistivity with temperature. We should notice though that the magnitudes of the effects, necessary to explain temperature-dependent magnetization, by far exceed the magnitude of the ρ_c variation observed in our experiments. This is also true with respect to doping evolution of the characteristic temperatures, T_{PG} in NMR measurements and T_{CG} in our resistivity measurements, Fig. 5, which do not connect gradually. Simultaneously the linear rise in magnetization with temperature does not coincide with resistivity maximum in our study, especially for pure BaFe_2As_2 .

Despite this clear discrepancy between the two suggested explanations for the temperature-dependent magnetization and transport and our data, the effects in the interplane resistivity and in the magnetization are clearly correlated. In addition, determination of the characteristic pseudogap temperature T_{PG} in NMR measurements is heavily model dependent, whereas the minimum in the temperature dependence of the interplane resistivity, despite being broad, is rather well defined for $x > 0.166$ and shows a systematic evolution. This may imply that we need to invoke different

mechanisms for the explanation of the pseudogap features in magnetic system and charge system probing measurements.

D. Maximum in the temperature-dependent interplane resistivity at T^*

The decrease in the interplane resistivity below T^* shows a clear correlation with the NMR Knight shift, therefore we need to look for a common origin. An important observation is that in BaCo122 with $x=0.08$, Fig. 6, both the Knight shift and the interplane resistivity at low temperatures, $T < T^*$, follow expectations of a metal with temperature-independent density of states: the resistivity shows metallic decrease on cooling and the Knight shift is temperature independent. Simultaneously, the $\frac{1}{T}$ increase indicates slowing down of magnetic fluctuations. This suggests that magnetic correlations may play an important role in the anomalies in all three measurements. Same trend holds for sample with $x=0.105$, however, the features in NMR measurements fade away with overdoping.

In the NMR study of Ref. 17, the temperature-dependent Knight shift was fit using a two-component model with $K = A + B \exp(-T_{PG}/T)$. At temperatures $T \ll T_{PG}$ this crosses over to a metallic behavior with constant Knight shift determined by the A term unaffected by the pseudogap. At $T > T_{PG}$ both terms become temperature independent and we can expect restoration of the metallic behavior with $K = A + B$. Fitting the temperature-dependent Knight shift, the authors determined $T_{PG} = 560 \text{ K} \pm 150 \text{ K}$ for optimally doped BaCo122 samples, $x=0.08$ (with $A=0.715\%$ and $B=0.244\%$), Ref. 17, and $T_{PG}=450 \text{ K}$ for $x=0.26$ (with $A=0.20\%$ and $B=0.23\%$). Assuming that the A and B coefficients represent partial DOS contributions of the ungapped and gapped parts of the Fermi surface, respectively, we would expect that at temperatures on the order of $T_{PG}/3$ or so, which would give us a temperature in 100–200 K range for optimal doping, we restore metallic resistivity temperature dependence, while resistivity decrease with temperature would be observed at higher temperatures due to carrier activation. This is consistent within general trend in evolution of $\rho_c(T)$, but not $\rho_a(T)$. This would suggest that the pseudogap affects predominantly the most warped parts of the Fermi surface.

We need to notice though, that it is difficult to explain resistivity decrease above T^* by the existence of a gap only for magnetic excitations or *spin gap*, as probed by NMR.³⁶ Activation of spin fluctuations in the metallic phase can only increase scattering of charge carriers, which is seen in in-plane transport. Decrease of the interplane resistivity, despite being very small, would require rather an increase in the carrier density by excitations over a *charge gap*.

E. Critical concentration

We now turn to the evolution of $\rho_c(T)$ and magnetic susceptibility in the vicinity of x_{CG} . The most remarkable observation here is that at $x=0.313$ the resistivity is fairly linear over a broad temperature range from approximately 400 K down to 20 K and saturates at lower temperatures. For x

$=0.290$ the dependence is also close to T linear with a shallow slope change at ~ 150 K. For doping with $x > 0.313$ the $\rho_c(T)$ becomes superlinear, similar to $\rho_a(T)$, and its inelastic part can be reasonably described as a sum of T linear and T^2 terms, as shown for the curves $x=0.343$ and $x=0.370$. In general, evolution of $\rho_c(T)$ with doping is reminiscent of the one found in systems on the verge of magnetic order and assigned to the existence of the magnetic quantum-critical point. This observation suggests that the pseudogap is magnetic in origin, and is accompanied by the charge gap, rather than the charge gap itself being responsible for anomalous electronic properties.

Of note, none of the anomalies in the magnetic properties is clearly reflected in the in-plane transport. This unusual single-axis effect of the pseudogap on the resistivity suggests that the magnetic action is concentrated on a small fraction of the Fermi surface, and importantly, on the most warped part contributing mainly to the interplane transport.

F. Origin of the pseudogap

The existence of two additional crossover lines in the phase diagram of $\text{Ba}(\text{Fe}_{1-x}\text{Co}_x)_2\text{As}_2$, as revealed by the interplane resistivity, raises an interesting question about their origins. Strong anisotropy of the pseudogap makes a scenario, in which the gap is due to superconducting pairing of charge carriers, however without superconducting condensate formation, very unlikely. We therefore should consider the possibility that the pseudogap is arising due to either short range, or short-lived, magnetic correlations, or represents a partial gap in the electronic structure.

The magnetic structure of parent BaFe_2As_2 is characterized by a stripe-type antiferromagnetic ordering, in which antiferromagnetic spin arrangement is typical for directions both in the plane and between the planes, introducing three-dimensional magnetic Brillouin zone, poorly matching the Fermi surface. It is difficult to expect pronounced anisotropy for this case. On the other hand, if correlations seen by the interplane transport were the same as those of the ordered phase, it would be difficult to explain a pretransition *decrease* in resistivity below T^* in Co-doped samples with $x = 0.037-0.058$, with successive *increase* in resistivity below T_{SM} . This may suggest that uniaxial anisotropy of the pseudogap comes from magnetic fluctuations with a different characteristic wave vector. A situation like this, when fluctuations and ordering wave vector are not the same was found in some intermetallic and heavy fermion systems.⁵³ Indirect evidence for such a possibility comes from the fact that in a closely related EuFe_2As_2 , antiferromagnetic ordering of Eu moments happens between the planes, while the Fe layer moments remain parallel in the planes.^{54,55} Since this ordering is mediated by Ruderman-Kittel-Kasuya-Yosida (RKKY) interactions via conduction electrons, it suggests that the generalized spin susceptibility may have maxima, which correspond to the existence of the interplane nesting.

In closely related BaMn_2As_2 , magnetism is of local moment type, and the magnetic order is of usual AF G -type.⁵⁶ In EuRh_2As_2 , commensurate and incommensurate spiral-like structures with propagation along the c axis are found.⁵⁷ Al-

though these compounds are differing in band structure and electron count, these observations of different types of ordering may be suggesting that various magnetic structures are not very different in energy.

In the lack of any evidence for the existence of such correlations in Co-doped BaFe_2As_2 , we just speculate what consequences uniaxial character of the pseudogap may have. This type of a pseudogap is impossible in two-dimensional cuprates, it is a direct consequence of the difference in the dimensionality of the electronic and magnetic systems in the cuprates and in iron arsenides. If the link between the symmetry of the pseudogap and of the superconducting order parameter, as found in the cuprates,^{3,58} is preserved in the iron arsenides, c -axis pseudogap would correspond to a superconducting gap having maxima/minima at the poles. This scenario was invoked theoretically for explanation of unusual behavior in the superconducting gap.⁵⁹ In experiment, variation in the superconducting gap with polar angle is found in inelastic neutron scattering in Ni-doped compound at optimal doping,⁶⁰ with gap magnitude decreasing toward the poles, and in penetration depth study of $\text{BaNi}122$.⁶¹ It is directly revealed in the interplane heat-transport study,²⁹ as opposed to the in-plane study.⁶²

Finally we would like to point to a certain similarity in the critical behavior of the interplane resistivity in $\text{BaCo}122$ and in CeCoIn_5 . In CeCoIn_5 , a true critical behavior at a field-tuned quantum critical point (Refs. 63 and 64) with T -linear resistivity and violation of the Wiedemann-Franz law is observed for transport along the tetragonal c axis.⁶⁵ Transport in the plane perpendicular to c axis, despite showing unusual power law behavior, obeys the Wiedemann-Franz law.⁶⁶

IV. CONCLUSION

Contrary to the in-plane electrical resistivity, which away from the domain of structural/magnetic ordering shows monotonic metallic temperature dependence, interplane resistivity, $\rho_c(T)$, reveals anomalous features clearly correlating with features in the temperature dependence of the NMR Knight shift and spin-relaxation rate, assigned to the formation of the pseudogap. Evolution of $\rho_c(T)$ with doping reveals two characteristic energy scales, of the resistivity maximum (seen for compositions $0 \leq x < \sim 0.2$) and resistivity minimum at a temperature T_{CG} , seen for $0.166 \leq x < x_c$, $x_c \approx 0.3$. The temperature-dependent ρ_c is close to linear close to x_{CG} and superlinear for $x > x_{CG}$. None of these features are evident in the in-plane resistivity $\rho_a(T)$. For doping levels $x < x_{CG}$, $\chi(T)$ shows a known, anomalous, T -linear dependence, which disappears for $x > x_{CG}$. These features are consistent with the existence of a partial gap on the Fermi surface (charge gap) accompanying formation of the magnetic pseudogap, and its critical suppression with doping. This evolution suggests existence of critical point for pseudogap order. The superconducting dome is confined inside the pseudogap dome.

Note added in proof: Recently a neutron scattering study found two-dimensional magnetic fluctuations in parent $\text{Ba}122$ in good match with pseudogap feature in interplane resistivity.⁶⁷

ACKNOWLEDGMENTS

We thank A. Kaminski and A. Kreyssig for useful discussions. Work at the Ames Laboratory was supported by the

Department of Energy-Basic Energy Sciences under Contract No. DE-AC02-07CH11358. R.P. acknowledges support from Alfred P. Sloan Foundation.

*Corresponding author; tanatar@ameslab.gov

- ¹J. G. Bednorz and K. A. Muller, *Rev. Mod. Phys.* **60**, 585 (1988).
- ²T. Timusk and B. Statt, *Rep. Prog. Phys.* **62**, 61 (1999).
- ³T. Kondo, R. Khasanov, T. Takeuchi, J. Schmalian, and A. Kaminski, *Nature (London)* **457**, 296 (2009).
- ⁴M. R. Norman, D. Pines, and C. Kallin, *Adv. Phys.* **54**, 715 (2005).
- ⁵V. Hinkov, P. Bourges, S. Pailhes, Y. Sidis, A. Ivanov, C. D. Frost, T. G. Perring, C. T. Lin, D. P. Chen, and B. Keimer, *Nat. Phys.* **3**, 780 (2007).
- ⁶K. K. Gomes, A. N. Pasupathy, A. Pushp, S. Ono, Y. Ando, and A. Yazdani, *Nature (London)* **447**, 569 (2007).
- ⁷N. P. Armitage, P. Fournier, and R. L. Greene, *Rev. Mod. Phys.* **82**, 2421 (2010).
- ⁸Y. Kamihara, T. Watanabe, M. Hirano, and H. Hosono, *J. Am. Chem. Soc.* **130**, 3296 (2008).
- ⁹I. I. Mazin, *Nature (London)* **464**, 183 (2010).
- ¹⁰Y. Kohama, Y. Kamihara, S. A. Baily, L. Civale, S. C. Riggs, F. F. Balakirev, T. Atake, M. Jaime, M. Hirano, and H. Hosono, *Phys. Rev. B* **79**, 144527 (2009).
- ¹¹K. Ahilan, F. L. Ning, T. Imai, A. S. Sefat, R. Jin, M. A. McGuire, B. C. Sales, and D. Mandrus, *Phys. Rev. B* **78**, 100501(R) (2008).
- ¹²Y. Nakai, S. Kitagawa, K. Ishida, Y. Kamihara, M. Hirano, and H. Hosono, *New J. Phys.* **11**, 045004 (2009); Y. Ishida, T. Shimojima, K. Ishizaka, T. Kiss, M. Okawa, T. Togashi, S. Watanabe, X.-Y. Wang, C.-T. Chen, Y. Kamihara, M. Hirano, H. Hosono, and S. Shin, *Phys. Rev. B* **79**, 060503 (2009).
- ¹³T. Sato, S. Souma, K. Nakayama, K. Terashima, K. Sugawara, T. Takahashi, Y. Kamihara, M. Hirano, and H. Hosono, *J. Phys. Soc. Jpn.* **77**, 063708 (2008).
- ¹⁴A. L. Solovjov, S. L. Sidorov, V. Yu. Tarenkov, and A. I. D'yachenko, *Low Temp. Phys.* **35**, 826 (2009).
- ¹⁵Y. Xu, P. Richard, K. Nakayama, T. Kawahara, Y. Sekiba, T. Qian, M. Neupane, S. Souma, T. Sato, T. Takahashi, H. Luo, H. Wen, G. Chen, N. Wang, Z. Wang, Z. Fang, X. Dai, and H. Ding, [arXiv:0905.4467](https://arxiv.org/abs/0905.4467) (unpublished).
- ¹⁶K. Ishida, Y. Nakai, and H. Hosono, *J. Phys. Soc. Jpn.* **78**, 062001 (2009).
- ¹⁷F. L. Ning, K. Ahilan, T. Imai, A. S. Sefat, R. Jin, M. A. McGuire, B. C. Sales, and D. Mandrus, *J. Phys. Soc. Jpn.* **77**, 103705 (2008).
- ¹⁸Y. Sekiba, T. Sato, K. Nakayama, K. Terashima, P. Richard, J. H. Bowen, H. Ding, Y.-M. Xu, L. J. Li, G. H. Cao, Z.-A. Xu, and T. Takahashi, *New J. Phys.* **11**, 025020 (2009).
- ¹⁹N. Ni, M. E. Tillman, J.-Q. Yan, A. Kracher, S. T. Hannahs, S. L. Bud'ko, and P. C. Canfield, *Phys. Rev. B* **78**, 214515 (2008).
- ²⁰N. Doiron-Leyraud, P. Auban-Senzier, S. René de Cotret, C. Bourbonnais, D. Jérôme, K. Bechgaard, and L. Taillefer, *Phys. Rev. B* **80**, 214531 (2009).
- ²¹M. A. Tanatar, N. Ni, C. Martin, R. T. Gordon, H. Kim, V. G. Kogan, G. D. Samolyuk, S. L. Bud'ko, P. C. Canfield, and R. Prozorov, *Phys. Rev. B* **79**, 094507 (2009).
- ²²M. A. Tanatar, N. Ni, G. D. Samolyuk, S. L. Bud'ko, P. C. Canfield, and R. Prozorov, *Phys. Rev. B* **79**, 134528 (2009).
- ²³M. A. Tanatar, E. C. Blomberg, A. Kreyssig, M. G. Kim, N. Ni, A. Thaler, S. L. Bud'ko, P. C. Canfield, A. I. Goldman, I. I. Mazin, and R. Prozorov, *Phys. Rev. B* **81**, 184508 (2010).
- ²⁴F. L. Ning, K. Ahilan, T. Imai, A. S. Sefat, R. Jin, M. A. McGuire, B. C. Sales, and D. Mandrus, *J. Phys. Soc. Jpn.* **78**, 013711 (2009).
- ²⁵N. D. Mathur, F. M. Grosche, S. R. Julian, I. R. Walker, D. M. Freye, R. K. W. Haselwimmer, and G. G. Lonzarich, *Nature (London)* **394**, 39 (1998).
- ²⁶M. A. Tanatar, N. Ni, S. L. Bud'ko, P. C. Canfield, and R. Prozorov, *Supercond. Sci. Technol.* **23**, 054002 (2010).
- ²⁷R. Prozorov, N. Ni, M. A. Tanatar, V. G. Kogan, R. T. Gordon, C. Martin, E. C. Blomberg, P. Prommapan, J. Q. Yan, S. L. Bud'ko, and P. C. Canfield, *Phys. Rev. B* **78**, 224506 (2008).
- ²⁸N. E. Hussey, K. Nozawa, H. Takagi, S. Adachi, and K. Tanabe, *Phys. Rev. B* **56**, R11423 (1997).
- ²⁹J.-Ph. Reid, M. A. Tanatar, X. G. Luo, H. Shakeripour, N. Doiron-Leyraud, N. Ni, S. L. Bud'ko, P. C. Canfield, R. Prozorov, and L. Taillefer, *Phys. Rev. B* **82**, 064501 (2010).
- ³⁰M. A. Tanatar, T. Ishiguro, H. Tanaka, and H. Kobayashi, *Phys. Rev. B* **66**, 134503 (2002).
- ³¹F. Rullier-Albenque, D. Colson, A. Forget, and H. Alloul, *Phys. Rev. Lett.* **103**, 057001 (2009).
- ³²E. D. Mun, S. L. Bud'ko, N. Ni, A. N. Thaler, and P. C. Canfield, *Phys. Rev. B* **80**, 054517 (2009).
- ³³C. Liu, T. Kondo, R. M. Fernandes, A. D. Palczewski, E. D. Mun, N. Ni, A. N. Thaler, A. Bostwick, E. Rotenberg, J. Schmalian, S. L. Bud'ko, P. C. Canfield, and A. Kaminski, *Nat. Phys.* **6**, 419 (2010).
- ³⁴F. L. Ning, K. Ahilan, T. Imai, A. S. Sefat, M. A. McGuire, B. C. Sales, D. Mandrus, P. Cheng, B. Shen, and H.-H. Wen, *Phys. Rev. Lett.* **104**, 037001 (2010).
- ³⁵J. Chu, J. Analytis, K. De Greve, P. McMahon, Z. Islam, Y. Yamamoto, and I. Fisher, *Science* **329**, 824 (2010).
- ³⁶K. Ahilan, F. L. Ning, T. Imai, A. S. Sefat, M. A. McGuire, B. C. Sales, D. Mandrus, P. Cheng, B. Shen, and H.-H. Wen, *Physica C* (to be published), [arXiv:0910.1071](https://arxiv.org/abs/0910.1071).
- ³⁷X. F. Wang, T. Wu, G. Wu, H. Chen, Y. L. Xie, J. J. Ying, Y. J. Yan, R. H. Liu, and X. H. Chen, *New J. Phys.* **11**, 045003 (2009).
- ³⁸J.-Q. Yan, A. Kreyssig, S. Nandi, N. Ni, S. L. Bud'ko, A. Kracher, R. J. McQueeney, R. W. McCallum, T. A. Lograsso, A. I. Goldman, and P. C. Canfield, *Phys. Rev. B* **78**, 024516 (2008).
- ³⁹R. Klingeler, N. Leps, I. Hellmann, A. Popa, U. Stockert, C. Hess, V. Kataev, H.-J. Grafe, F. Hammerath, G. Lang, S. Wurmehl, G. Behr, L. Harnagea, S. Singh, and B. Buchner, *Phys.*

- Rev. B* **81**, 024506 (2010).
- ⁴⁰N. Katayama, Y. Kiuchi, Y. Matsushita, and K. Ohguchi, *J. Phys. Soc. Jpn.* **78**, 123702 (2009).
- ⁴¹W. Malaeb, T. Yoshida, A. Fujimori, M. Kubota, K. Ono, K. Kihou, P. M. Shirage, H. Kito, A. Iyo, H. Eisaki, Y. Nakajima, T. Tamegai, and R. Arita, *J. Phys. Soc. Jpn.* **78**, 123706 (2009).
- ⁴²P. Vilmercati, A. Fedorov, I. Vobornik, U. Manju, G. Panaccione, A. Goldoni, A. S. Sefat, M. A. McGuire, B. C. Sales, R. Jin, D. Mandrus, D. J. Singh, and N. Mannella, *Phys. Rev. B* **79**, 220503 (2009).
- ⁴³C. Uffeld, J. Laverock, T. D. Haynes, S. B. Dugdale, J. A. Duffy, M. W. Butchers, J. W. Taylor, S. R. Giblin, J. G. Analytis, J.-H. Chu, I. R. Fisher, M. Itou, and Y. Sakurai, *Phys. Rev. B* **81**, 064509 (2010).
- ⁴⁴S. Thirupathiah, S. de Jong, R. Ovsyannikov, H. A. Dürr, A. Varykhalov, R. Follath, Y. Huang, R. Huisman, M. S. Golden, Y.-Z. Zhang, H. O. Jeschke, R. Valentí, A. Erb, A. Gloskovskii, and J. Fink, *Phys. Rev. B* **81**, 104512 (2010).
- ⁴⁵D. J. Singh, *Phys. Rev. B* **78**, 094511 (2008).
- ⁴⁶A. S. Sefat, R. Jin, M. A. McGuire, B. C. Sales, D. J. Singh, and D. Mandrus, *Phys. Rev. Lett.* **101**, 117004 (2008).
- ⁴⁷A. F. Kemper, C. Cao, P. J. Hirschfeld, and H.-P. Cheng, *Phys. Rev. B* **80**, 104511 (2009).
- ⁴⁸H. Wadati, I. Elfimov, and G. A. Sawatzky, [arXiv:1003.2663](https://arxiv.org/abs/1003.2663) (unpublished).
- ⁴⁹I. I. Mazin and M. D. Johannes, *Nat. Phys.* **5**, 141 (2009); M. D. Johannes and I. I. Mazin, *Phys. Rev. B* **79**, 220510 (2009).
- ⁵⁰L. Fang, H. Luo, P. Cheng, Z. Wang, Y. Jia, G. Mu, B. Shen, I. I. Mazin, L. Shan, C. Ren, and H.-H. Wen, *Phys. Rev. B* **80**, 140508(R) (2009).
- ⁵¹D. K. Pratt, W. Tian, A. Kreyssig, J. L. Zarestky, S. Nandi, N. Ni, S. L. Bud'ko, P. C. Canfield, A. I. Goldman, and R. J. McQueeney, *Phys. Rev. Lett.* **103**, 087001 (2009).
- ⁵²B. C. Sales, M. A. McGuire, A. S. Sefat, and D. Mandrus, *Physica C* **470**, 304 (2010).
- ⁵³See, for example, H. Lin, L. Rebelsky, M. F. Collins, J. D. Garrett, and W. J. L. Buyers, *Phys. Rev. B* **43**, 13232 (1991).
- ⁵⁴Y. Xiao, Y. Su, M. Meven, R. Mittal, C. M. N. Kumar, T. Chatterji, S. Price, J. Persson, N. Kumar, S. K. Dhar, A. Thamizhavel, and Th. Brueckel, *Phys. Rev. B* **80**, 174424 (2009).
- ⁵⁵J. Herrero-Martín, V. Scagnoli, C. Mazzoli, Y. Su, R. Mittal, Y. Xiao, Th. Brueckel, N. Kumar, S. K. Dhar, A. Thamizhavel, and L. Paolasini, *Phys. Rev. B* **80**, 134411 (2009).
- ⁵⁶Y. Singh, M. A. Green, Q. Huang, A. Kreyssig, R. J. McQueeney, D. C. Johnston, and A. I. Goldman, *Phys. Rev. B* **80**, 100403(R) (2009).
- ⁵⁷S. Nandi, A. Kreyssig, Y. Lee, Y. Singh, J. W. Kim, D. C. Johnston, B. N. Harmon, and A. I. Goldman, *Phys. Rev. B* **79**, 100407(R) (2009).
- ⁵⁸F. Ronning, C. Kim, D. L. Feng, D. S. Marshall, A. G. Loeser, L. L. Miller, J. N. Eckstein, I. Bozovic, and Z. X. Shen, *Science* **282**, 2067 (1998).
- ⁵⁹M. S. Laad and L. Craco, *Phys. Rev. Lett.* **103**, 017002 (2009).
- ⁶⁰S. Chi, A. Schneidewind, J. Zhao, L. W. Harriger, L. Li, Y. Luo, G. Cao, Zh. Xu, M. Loewenhaupt, J. Hu, and P. Dai, *Phys. Rev. Lett.* **102**, 107006 (2009).
- ⁶¹C. Martin, H. Kim, R. T. Gordon, N. Ni, V. G. Kogan, S. L. Bud'ko, P. C. Canfield, M. A. Tanatar, and R. Prozorov, *Phys. Rev. B* **81**, 060505(R) (2010).
- ⁶²M. A. Tanatar, J.-Ph. Reid, H. Shakeripour, X. G. Luo, N. Doiron-Leyraud, N. Ni, S. L. Bud'ko, P. C. Canfield, R. Prozorov, and L. Taillefer, *Phys. Rev. Lett.* **104**, 067002 (2010).
- ⁶³J. Paglione, M. A. Tanatar, D. G. Hawthorn, E. Boaknin, R. W. Hill, F. Ronning, M. Sutherland, L. Taillefer, C. Petrovic, and P. C. Canfield, *Phys. Rev. Lett.* **91**, 246405 (2003).
- ⁶⁴A. Bianchi, R. Movshovich, I. Vekhter, P. G. Pagliuso, and J. L. Sarrao, *Phys. Rev. Lett.* **91**, 257001 (2003).
- ⁶⁵M. A. Tanatar, J. Paglione, C. Petrovic, and L. Taillefer, *Science* **316**, 1320 (2007).
- ⁶⁶J. Paglione, M. A. Tanatar, D. G. Hawthorn, F. Ronning, R. W. Hill, M. Sutherland, L. Taillefer, and C. Petrovic, *Phys. Rev. Lett.* **97**, 106606 (2006).
- ⁶⁷S. D. Wilson, Z. Yamani, C. R. Rotundu, B. Freelon, P. N. Valdivia, E. Bourret-Courchesne, J. W. Lynn, S. Chi, T. Hong, and R. J. Birgeneau, *Phys. Rev. B* **82**, 1144502 (2010).